Journal of Materials Chemistry C

ROYAL SOCIETY OF CHEMISTRY

PAPER

View Article Online
View Journal

Check for updates

Cite this: DOI: 10.1039/d5tc04544d

Structure and electrical properties of Ga_2O_3 thin films grown by atomic layer deposition on Ru and TiN electrodes

Lauri Aarik, *[a] Aivar Tarre,[a] Hugo Mändar,[a] Joonas Merisalu,[a] Jun Lu,[b] Lars Hultman[bcd] and Jaan Aarik[a]

Received 30th December 2025,
Accepted 13th February 2026

DOI: 10.1039/d5tc04544d

rsc.li/materials-c

The composition, structure, and electrical properties of Ga_2O_3 thin films, grown by atomic layer deposition (ALD) from GaI_3 and O_3 precursors, were characterized. The films were deposited on Si substrates and on Ru and TiN bottom electrodes at temperatures of 200–500 °C. Growth of κ- and ε-Ga_2O_3 was observed on Ru and TiN at substrate temperatures ≥ 325 °C, while temperatures ≥ 425 °C were needed to deposit crystalline Ga_2O_3 on bare Si. The formation of both ε-Ga_2O_3 and predominant κ-Ga_2O_3 phases in crystalline films was confirmed by high-resolution transmission electron microscopy studies. Films deposited at 375–450 °C exhibited low leakage current densities (down to 10^{-9} A cm^{-2} at an electric field strength of 0.1 MV cm^{-1}), breakdown fields up to 6.5 MV cm^{-1}, and permittivity values up to 22 at 10 kHz. These results demonstrate that Ga_2O_3 deposited in this ALD process is suitable for implementation as high permittivity dielectrics in advanced electronic devices. Furthermore, the findings highlight the importance of deposition temperature and substrate choice in optimizing the dielectric properties of Ga_2O_3 films deposited for these applications.

1. Introduction

Gallium oxide (Ga_2O_3) is a wide-bandgap semiconductor with promising potential in many important applications.[1–5] For example, the possibility of using Ga_2O_3 as a wide-bandgap material in radiation detectors,[6,7] chemical sensors,[8,9] and high-power electronic devices[3,10,11] has been demonstrated. In addition, since the conductivity of Ga_2O_3 can be varied in a wide range, thin films of this material have been employed as dielectrics in resistive switching metal–insulator–metal structures[12] as well as transparent conducting electrodes for optoelectronic devices.[13]

Ga_2O_3 has been obtained in α, β, γ, δ, ε, κ, and amorphous phases, exhibiting markedly different properties. For instance, one can find densities of 4.98–5.18 g cm^{-3} for cubic (space group $Ia\bar{3}$) δ-Ga_2O_3[1] and 6.48 g cm^{-3} for rhombohedral ($R\bar{3}c$) α-Ga_2O_3[1] in the literature. Similarly, the relative permittivity (k) is phase dependent, with values reported to be 9.2–11.9 for amorphous Ga_2O_3,[14,15] 9.3–12.4 for monoclinic ($C2/m$) β-Ga_2O_3,[16–19] and 15–32 for the orthorhombic ($Pna2_1$) phase of Ga_2O_3.[20,21] Notably, in different publications, the orthorhombic phase of Ga_2O_3, which has been shown to exhibit the highest k values and therefore is of particular importance for some electronic applications, is referred to as κ-Ga_2O_3[21–23] and also as ε-Ga_2O_3.[20] This is likely because, in thin films, a structure consisting of 120° rotational nanoscale domains of orthorhombic κ-Ga_2O_3 results in an X-ray diffraction (XRD) pattern very similar to that of hexagonal ε-Ga_2O_3 (space group $P6_3mc$), making it difficult to distinguish these two phases.[22–25]

Owing to the strong dependence of material properties on its phase composition, selecting and stabilizing the most suitable phase for each application are important tasks. In thin films, the phase composition depends on the fabrication method, process parameters, and substrates used for deposition. For instance, previous publications have described the deposition of α-Ga_2O_3 on differently orientated sapphire[1,26] and α-Cr_2O_3;[25,27] monoclinic ($C2/m$) β-Ga_2O_3 on sapphire,[1] silicon,[28] MgO,[7] GaN,[29] TiN,[30] Pt,[19] and Ru;[31] hexagonal ($P6_3mc$) ε-Ga_2O_3 and/or orthorhombic ($Pna2_1$) κ-Ga_2O_3 on c-cut sapphire,[23,24] silicon,[25] yttria-stabilized zirconia,[32] MgO,[32] GaN,[33,34] SiC,[34] AlN,[33,35] $MgAl_2O_4$,[35] $SrTiO_3$,[36] indium-tin oxide,[20] and Pt;[21] cubic ($Fd\bar{3}m$) γ-Ga_2O_3 on $MgAl_2O_4$,[26,35] MgO,[35] and GaN;[35] δ-Ga_2O_3 on β-Fe_2O_3.[37] Earlier studies also demonstrated that the choice of deposition

[a] Institute of Physics, University of Tartu, W. Ostwaldi 1, 50411 Tartu, Estonia. E-mail: lauri.aarik@ut.ee
[b] Thin Film Physics Division, Department of Physics, Chemistry and Biology (IFM), Linköping University, SE-581 83 Linköping, Sweden
[c] Wallenberg Initiative Material Science for Sustainability, Thin Films Physics Division, Department of Physics (IFM), Linköping University, SE 581 83 Linköping, Sweden
[d] Center for Plasma and Thin Film Technologies, Ming Chi University of Technology, 84 Gungjuan Rd., Taishan Dist., New Taipei City 24301, Taiwan

temperature,[26,34,35] deposition method,[21,28] precursors, and precursor dosing[35] is of comparable importance in the stabilization of selected crystalline phases during the thin-film growth.

Besides several other material properties, the concentration of residual impurities, which in turn affects the charge carrier concentration and transport in semiconductors and dielectrics, may also depend on the phase composition. For example, the concentration of residual impurities has been lower in the rutile-phase TiO_2 grown by atomic layer deposition (ALD) on RuO_2 electrodes than in the anatase films obtained on the Si(100) surface in the same ALD process at the same temperature.[38] Lower concentrations of impurities were also obtained in orthorhombic $Hf_xTi_{1-x}O_y$ grown on Ru seed layers compared with amorphous $Hf_xTi_{1-x}O_y$ deposited on Pt and Si(100) at the same process parameters.[39] Studies on ALD of Ga_2O_3 from GaI_3 and O_3, yielding amorphous and $\kappa(\varepsilon)$ modifications of Ga_2O_3 on silicon and α-Ga_2O_3 on α-Cr_2O_3 seed layers,[25] gave a similar result. The α-Cr_2O_3 seed layers, supporting the formation of a high-density α-Ga_2O_3 phase, simultaneously resulted in lower concentrations of impurities in the Ga_2O_3 films.[25]

In previous studies, Ga_2O_3 films grown on the surfaces of dielectrics or semiconductors have mainly been characterized. Only a limited number of publications have described the growth of Ga_2O_3 on highly conductive electrode materials.[19–21,30,31] However, in many electronic applications, the deposition of wide-gap semiconductors and dielectrics on materials with high (metallic) conductivity is required. Motivated by this need, the present study investigates the ALD of Ga_2O_3 on TiN- and Ru-coated substrates and examines how these electrode materials influence the properties of Ga_2O_3 films. The main task was to evaluate how well our novel GaI_3- and O_3-based ALD process[25,27] is suited for the deposition of Ga_2O_3 on these electrode materials.

Although oxidation of the bottom electrode during O_3-based ALD was anticipated, TiN was selected due to its widespread use in semiconductor devices. Ru, which forms conductive oxides, was included as an alternative electrode material to mitigate the oxidation-related decrease in the bottom electrode conductivity.

The results presented in this report demonstrate that crystalline Ga_2O_3 can be obtained on both TiN and Ru at significantly lower temperatures than on uncoated silicon substrates. This enabled us to investigate the influence of substrates on crystal growth and to better understand the effect of crystallization on the growth per cycle (GPC) and other characteristics of thin films deposited in this ALD process. Most importantly, this study provides new insights into how the phase composition influences the electrical properties of Ga_2O_3, which is crucial for its implementation in devices such as field effect transistors and different types of memories based on metal–dielectric–semiconductor and metal–dielectric–metal structures.

2. Experimental details

The Ga_2O_3 films were deposited on bare Si(100) and on Ru- and TiN-coated Si(100) substrates using a flow type ALD reactor described previously.[40] The Ru and TiN coatings were deposited by magnetron sputtering and pulsed chemical vapor deposition techniques, respectively. For the deposition of Ga_2O_3 films, ALD cycles including a GaI_3 vapor pulse, purge, ozone pulse, and another purge, each with a duration of 2 s, were used. Sufficient vapor pressure of GaI_3 was obtained by heating GaI_3 powder (99%, Strem Chemicals, Inc) at 130 °C. Ozone was generated from O_2 (99.999%, AS Linde Gas). The Ga_2O_3 films were deposited applying 700 ALD cycles at T_G of 200–500 °C and 250 cycles at 325–500 °C. Other details of the ALD process are described in our previous publication.[25]

The elemental compositions and mass thicknesses of films were measured with an X-ray fluorescence (XRF) spectrometer ZSX-400 (Rigaku). The phase composition was characterized by grazing incidence X-ray diffraction (GIXRD) using an X-ray diffractometer Smartlab (Rigaku) working at a tube power of 8.1 kW (CuKα radiation). The X-ray diffraction database PDF-2 of the International Centre of Diffraction Data (version 2020) was used for qualitative phase analysis. The thickness, density, and surface roughness were calculated from the X-ray reflectometry (XRR) results recorded with the same X-ray diffractometer. Additionally, the thickness values were measured using a GES-5E (Sopra-Semilab) spectroscopic ellipsometer (SE).

High-angle annular dark-field (HAADF) STEM imaging, and EDX analysis were performed using a double-corrected FEI Titan3 S/TEM, operated at 300 kV, equipped with a Super-X EDX detector. TEM imaging and selective area electron diffraction (SAED) were performed on a FEI Tecnai G2 TEM operated at 200 kV. FFT patterns of TEM images were indexed using program CrysTBox.[41]

The top electrodes needed for the electrical characterization of Ga_2O_3 were fabricated by electron beam evaporation of Pt through a shadow mask. The sizes of circular top electrodes were determined by diameters of the mask openings (50, 250, and 500 μm), while the thicknesses of the electrodes were around 50 nm. Electrical characteristics were measured using a light-proof and electrically shielded Cascade Microtech MPS150 probe station, Keithley 2636A source-meter and Agilent E4980A LCR analyzer. Capacitance was measured at frequencies ranging from 5 kHz to 2 MHz.

3. Results and discussion

3.1. Composition and structure

According to the results of XRF studies, the O/Ga atomic ratio was 1.5 ± 0.1 in the samples with films grown applying 700 ALD cycles on bare Si substrates at 200–500 °C, on TiN bottom electrodes at 275–450 °C, and on Ru bottom electrodes at 275 °C (Fig. S1). With the decrease of T_G down to 200 °C and its increase up to 500 °C, the O/Ga ratio gradually rose reaching 1.7 ± 0.1 in the samples where these films were grown on Ru and TiN at 200 °C, and on TiN at 500 °C. In the case of films grown with 700 cycles on Ru and with 250 cycles on TiN, the mean O/Ga ratio increased from 1.6 ± 0.1 to 2.1 ± 0.1 with the T_G increase from 325 to 500 °C. An even steeper increase in

the O/Ga ratio (from 1.6 to 2.5) was observed for films grown with 250 cycles on Ru as T_G increased from 325 to 500 °C (Fig. S1). As the characteristic X-ray emission recorded in our XRF studies was emitted from the material layer that was much thicker than the Ga_2O_3/Ru and Ga_2O_3/TiN stacks, the O/Ga ratio determined from the XRF data also depended on the amount of oxygen absorbed by the Ru and TiN layers. Therefore, the increase in O/Ga ratio with increasing T_G and decreasing film thickness was evidently caused by the oxidation of Ru and TiN surfaces at higher T_G as confirmed by the TEM and STEM data presented in Fig. 1 for Ga_2O_3 deposited at 450 °C on Ru (Fig. 1a and b) and TiN (Fig. 1c and d).

The STEM-EDX line scans across the Ga_2O_3/Ru and Ga_2O_3/TiN/Si interfaces revealed that a RuO_x layer with a thickness of around 4 nm was formed on Ru in the former structure (Fig. 1b) while TiO_xN_y was formed as a result of TiN oxidation throughout the bottom electrode in the latter case (Fig. 1d). The O peak at the interface between TiO_xN_y and the Si substrate in Fig. 1d probably comes from the native SiO_2 layer.

The XRF data demonstrate that the concentration of residual iodine impurities, which remained in the Ga_2O_3 films because of incomplete removal of Ga precursor ligands in the ALD process, decreased to 10^{-2} at% with the increase of T_G to 375–500 °C (Fig. 2). At T_G of 275–400 °C, the iodine concentrations were slightly lower in the films deposited on Ru and TiN than in the films deposited on bare Si at the same temperatures. However, the difference did not exceed the experimental uncertainty (Fig. 2).

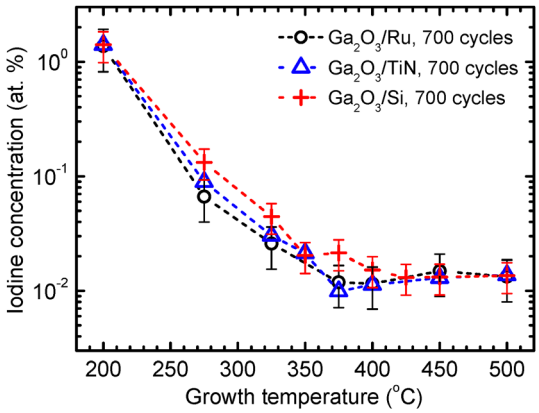

Fig. 2 Iodine concentration as a function of T_G in Ga_2O_3 films deposited on Ru, TiN, and bare silicon using 700 ALD cycles.

GIXRD studies revealed the presence of crystalline Ga_2O_3 in the films grown on Ru and TiN with 250 ALD cycles at $T_G \geq 350$ °C and with 700 cycles at $T_G \geq 325$ °C (Fig. 3). All films deposited on Ru and TiN at lower T_G values (Fig. 3), similar to the films deposited on bare Si substrates at $T_G < 425$ °C,[25,27]

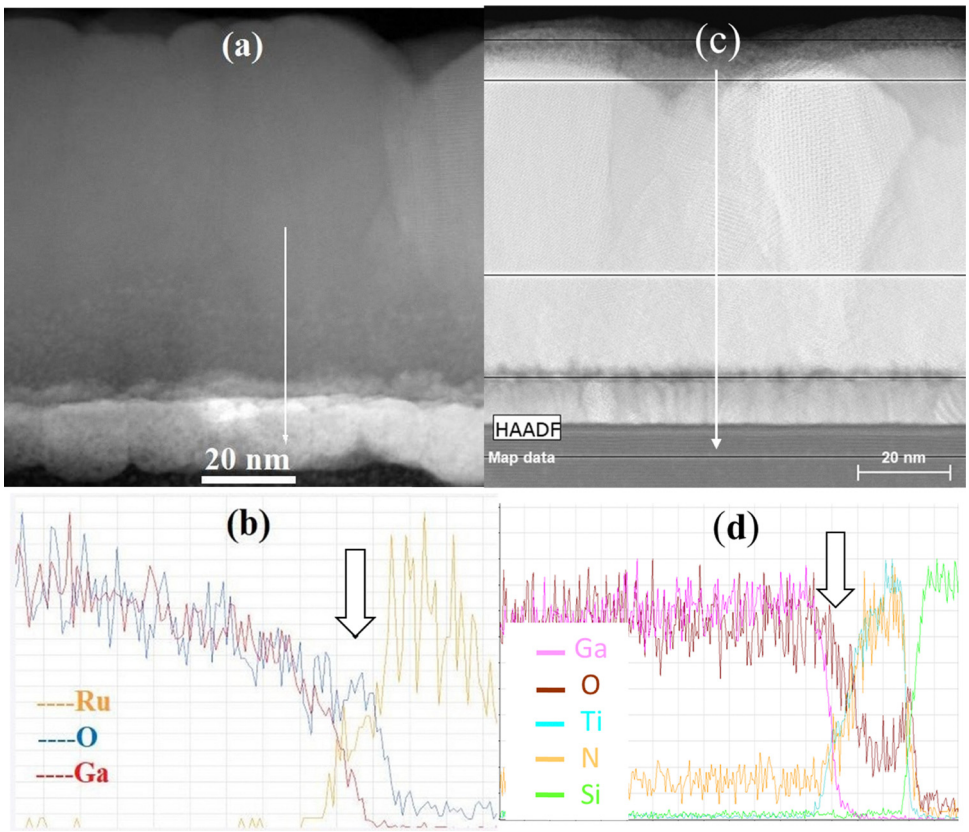

Fig. 1 (a) and (c) HRTEM images and (b) and (d) elemental composition profiles determined by STEM-EDX for Ga_2O_3 films deposited on (a) and (b) Ru- and (c) and (d) TiN-coated silicon substrates at 450 °C. The arrows indicate (a) and (c) the ranges and directions of STEM-EDX scans, and (b) and (d) the interface between Ga_2O_3 and the bottom electrode.

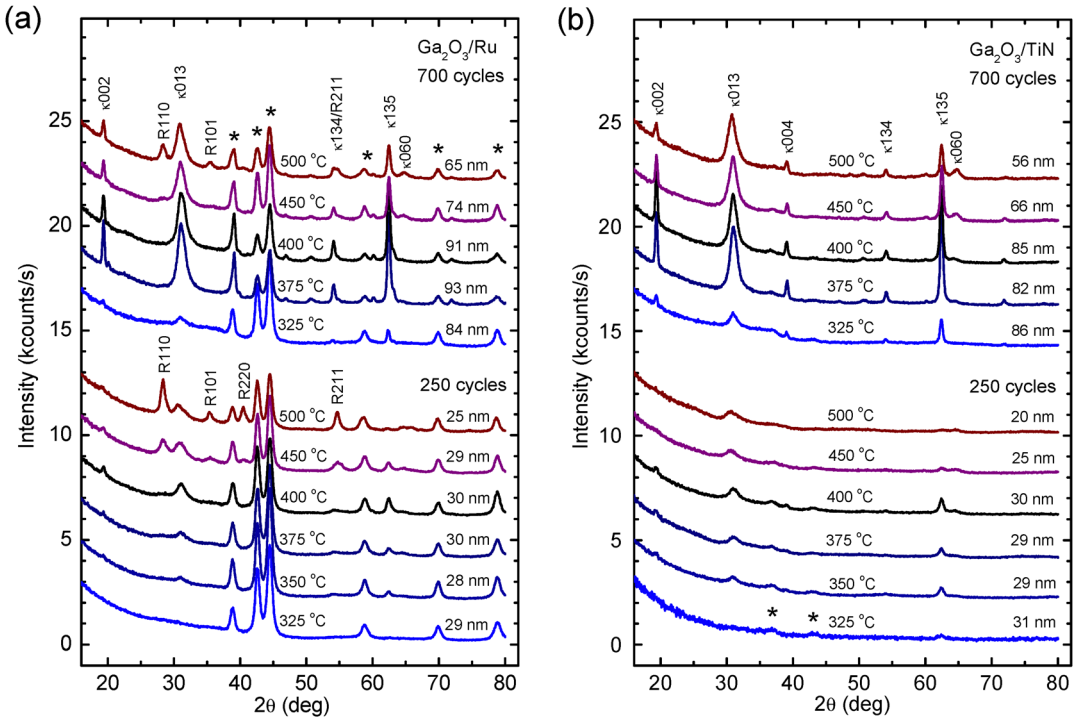

Fig. 3 Grazing incidence X-ray diffractograms of Ga_2O_3 films deposited on (a) Ru and (b) TiN-at different temperatures using 250 and 700 ALD cycles. The growth temperatures and thicknesses of films are shown at corresponding diffractograms. Miller indices of κ-Ga_2O_3 (κ) and rutile-phase RuO_2 (R) are shown at respective reflections. The reflections marked with asterisk (*) originate from (a) Ru and (b) TiN.

were amorphous. Comparison of diffractograms depicted in Fig. 3 with XRD databases indicated that κ-Ga_2O_3 was formed in the crystalline films. This conclusion is based on reflections peaking at 19.4°, 31.0°, 54.1°, and 62.4° (Fig. 3a and b). These reflections belong to κ-Ga_2O_3 and can be indexed as 002, 013, 134, and 135, respectively. In addition, a reflection at 39.1° in the diffractograms of films grown on TiN (Fig. 3b) was identified as the 004 reflection of κ-Ga_2O_3. However, it is possible that the ε-Ga_2O_3 phase was also present in the films because the reflections peaking at 19.4°, 54.1°, and 62.4° may also be attributed to this phase.

In the diffraction patterns of samples with Ga_2O_3 films grown on Ru at $T_G \geq 375$ °C, reflections attributable to the rutile phase of RuO_2 can also be seen at 28.3°, 35.3°, 40.4°, and 54.6° (Fig. 3a). The intensities of these reflections increase with increasing T_G and decreasing film thickness. Therefore, the GIXRD results confirm the STEM-EDX data (Fig. 1b) indicating that a RuO_2 interface layer was formed on Ru during the initial stage of Ga_2O_3 deposition at higher T_G. Although the oxidation of TiN was also evident from the STEM results (Fig. 1d), no reflections of crystalline TiO_2 phases appeared in the GIXRD patterns of samples with Ga_2O_3 films grown on TiN at temperatures up to 500 °C (Fig. 3b). However, crystalline TiO_2 (anatase) was observed in the samples containing Ga_2O_3 deposited at 550 °C (Fig. S2).

With the increase of T_G to 450–500 °C, a reflection at 64.6°–64.8° and a reflection tale at 31.5°–32.0° appeared in the GIXRD patterns (Fig. 3a and b). A possible reason for these changes could be the formation of β-Ga_2O_3 in addition to κ/ε-Ga_2O_3 in the films deposited at higher T_G. As shown in Fig. S2, a significant number of β-Ga_2O_3 reflections can be indexed in the diffractogram of a Ga_2O_3 film deposited on TiN at 550 °C. Therefore, in a T_G range of 450–500 °C, a transition from the growth of κ/ε-Ga_2O_3 to that of β-Ga_2O_3 started.

The data displayed in Fig. 3 also show that with increasing number of ALD cycles, the intensities of Ga_2O_3 GIXRD reflections increase faster than the film thicknesses do. Therefore, the crystallinity of the films improved during the deposition process either due to the crystallization of the amorphous material initially synthesized in the ALD reactions or because of increasing lateral sizes of crystallites with increasing film thickness. As can be seen in TEM images (Fig. 1) the latter reason seems to be more probable because the crystalline films contain pyramidal or conical grains with lateral sizes increasing with the distance from the film/substrate interface (Fig. 1c). Fig. 1c further shows that the material density in these grains is higher than that between the grains. Therefore, the grains evidently contain crystalline material as confirmed by the results of HRTEM studies presented in Fig. 4 and 5. Correspondingly, the increase in the lateral sizes of these grains with the increasing distance from the substrate surface means that the relative amount of crystalline material is higher at the top region of a film and in thicker films.

More information about the presence and location of different phases in crystalline Ga_2O_3 was obtained from HRTEM studies of a film deposited at 450 °C using 700 ALD cycles.

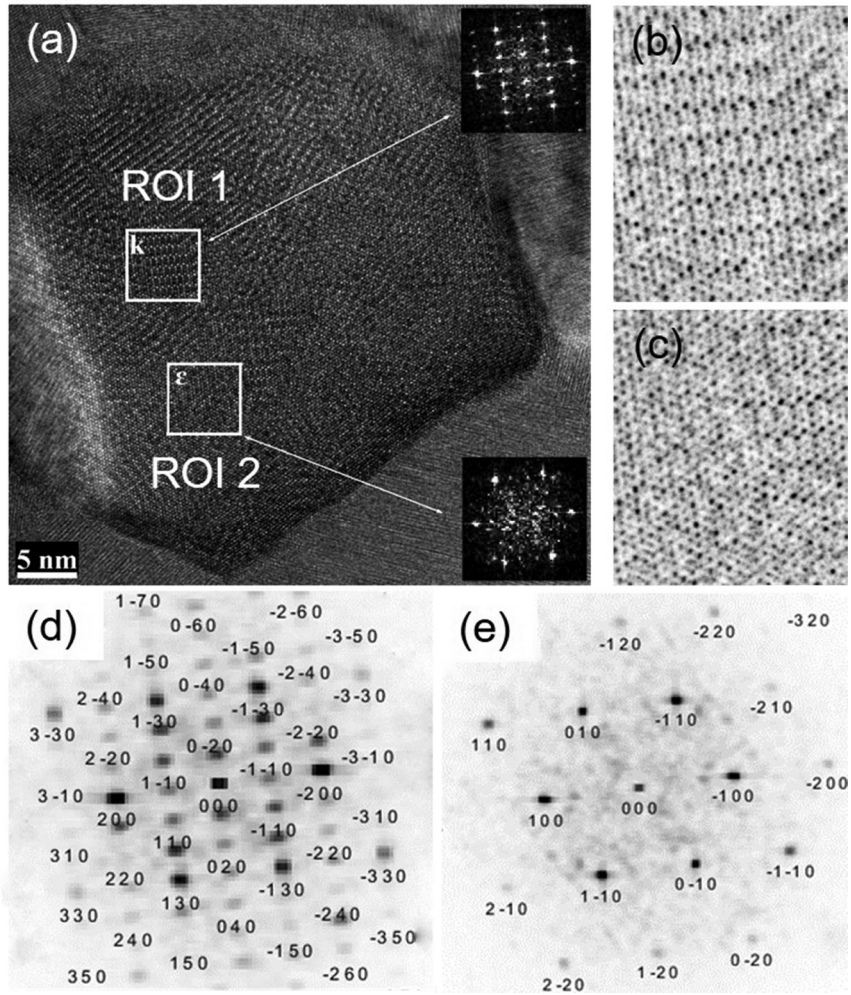

Fig. 4 (a) Top-view TEM image of a Ga_2O_3 grain showing ranges of interest ROI 1 and ROI 2 with different structures (denoted with κ and ε, respectively). (b) and (c) Enlarged high-resolution images of (b) ROI 1 and (c) ROI 2, and (d) and (e) FFT patterns of (d) ROI 1, indexed assuming lattice symmetry of κ-Ga_2O_3, and (e) ROI 2, indexed assuming lattice symmetry of ε-Ga_2O_3.

The κ-Ga_2O_3 phase that was identified in the films by XRD is orthorhombic with cell parameters of a = 5.0566 Å, b = 8.6867 Å, and c = 9.3035 Å, while ε-Ga_2O_3 has a hexagonal structure with lattice parameters a = 2.99 Å and c = 9.3 Å. In both crystal structures, the O atoms are arranged in a 4H (ABAC) close-packed stacking arrangement. The difference between the two structures is that in κ-Ga_2O_3, Ga atoms occupy tetrahedral (Ga_I) and octahedral (Ga_{II}, Ga_{III}, Ga_{IV}) sites, while in ε-Ga_2O_3, Ga atoms occupy octahedral and tetrahedral sites in a disordered manner. Previous work reported that κ-Ga_2O_3 and ε-Ga_2O_3 have crystal relationships $[0001]_\varepsilon//[001]_\kappa$, $[1010]_\varepsilon//[100]_\kappa$ and $[11-20]_\varepsilon//[010]_\kappa$.[23] Because the films have a strong fiber texture along the c axis, we can distinguish κ-Ga_2O_3 from ε-Ga_2O_3 in the Ga_2O_3 film with TEM in top-view along the c axis (Fig. 4) and in the cross-section from the $[1-100]_\varepsilon$ or $[100]_\kappa$ direction, but not from $[11-20]_\varepsilon$($[010]_\kappa$), as the HRTEM patterns are the same along the latter direction.

Fig. 4a shows a plan-view image of a Ga_2O_3 grain that consists of several nano-domains. High-resolution images and corresponding FFT patterns are presented in Fig. 4b–e. Most of the domains are κ-Ga_2O_3, as indicated by the high-resolution image (Fig. 4b) and corresponding FFT pattern (Fig. 4d). However, it was also possible to find a domain with a hexagonal structure (Fig. 4a and c), which was indexed as ε-Ga_2O_3 (Fig. 4e). In this domain, which has a diameter of around 5 nm, no 120° twin of κ-Ga_2O_3, described by Cora *et al.*,[23] was found. This result was confirmed by the convergent beam electron diffraction patterns (CBED) shown in Fig. S3a.

It is worth noting that the reflections observable in Fig. 4e can also be indexed as those of κ-Ga_2O_3 (Fig. S4). In this case, the standard deviation of fitting (Δd = 0.0010 nm) is even smaller than that for ε-Ga_2O_3 (Δd = 0.0012 nm). However, the absence of 110, 020, and 120 reflections of κ-Ga_2O_3 in the FFT pattern (Fig. S4) indicates that the domain contains ε-Ga_2O_3 rather than κ-Ga_2O_3.

The cross-sectional image in Fig. 5 shows a Ga_2O_3 grain, that mainly consists of κ-Ga_2O_3 but also contains a domain of ε-Ga_2O_3 co-growing with κ-Ga_2O_3 in the top region of the grain. The enlarged high-resolution images, corresponding FFT patterns, and SAED patterns of both phases are shown in

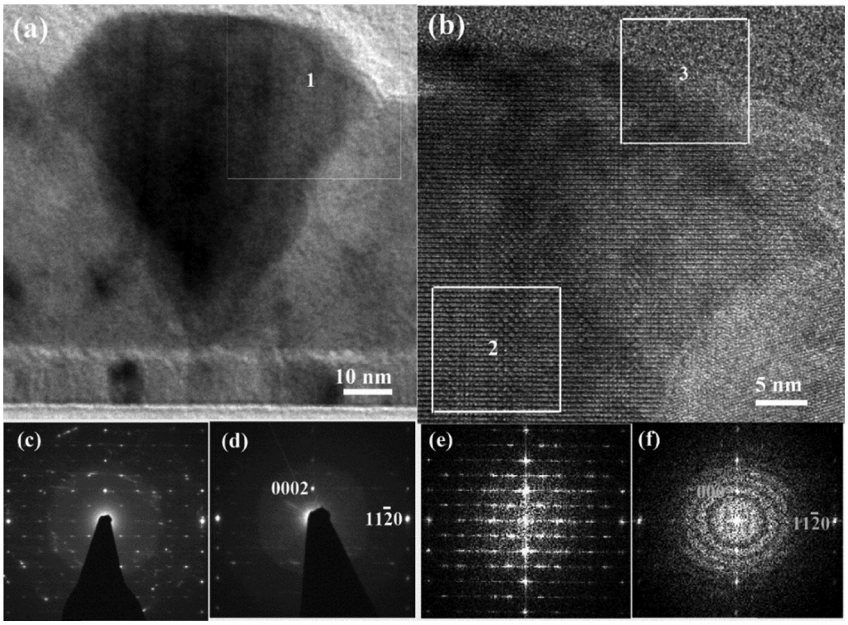

Fig. 5 Cross-sectional HRTEM of (a) one Ga_2O_3 grain and (b) an enlarged image of region 1 in panel (a) showing κ-Ga_2O_3 in box 2 and ε-Ga_2O_3 in box 3. (c) and (d) Electron diffraction patterns (SAED) and (e) and (f) FFT patterns of (c) and (e) κ-Ga_2O_3 from box 2 and (d) and (f) ε-Ga_2O_3 from box 3.

Fig. S5 and S6. These results confirm the growth of ε-Ga_2O_3 in addition to the predominant κ-Ga_2O_3. Furthermore, in the HRTEM studies, some Ga_2O_3 grains with space distance around 0.59 nm (Fig. 6), corresponding to the (200) plane of the β-Ga_2O_3 structure, were found. Therefore, the reflection peaking at 64.60°–64.80° in the GIXRD diffractograms of films deposited at $T_G > 450$ °C (Fig. 3) can be attributed to β-Ga_2O_3.

In the previous studies, κ-Ga_2O_3 was observed in films grown on bare silicon substrates at $T_G \geq 425$ °C.[25,27] Thus, the T_G values leading to the formation of κ-Ga_2O_3 and ε-Ga_2O_3 on Ru and TiN (Fig. 3) were about 100 °C lower than those required for crystallization of Ga_2O_3 on silicon. A reason for the lower crystallization temperatures on Ru and TiN could be a local epitaxial growth similar to that of TiO_2 on RuO_2.[42] However, no significant epitaxial relationship between Ga_2O_3 and Ru (RuO_2) or Ga_2O_3 and TiN (TiO_2) was found by TEM. Hence, there should be other reasons leading to more preferential crystallization of Ga_2O_3 on Ru and TiN than on silicon. For instance, rougher surfaces of Ru and TiN compared with the surface of bare silicon (Fig. 1) and the higher reactivity of GaI_3 towards Ru and TiN, leading to more efficient release of iodine ligands (Fig. 2), might contribute to the nucleation of Ga_2O_3. This conclusion is in line with the results of previous studies showing that an increase in surface roughness promoted more efficient nucleation of Ga_2O_3 on Ru.[31]

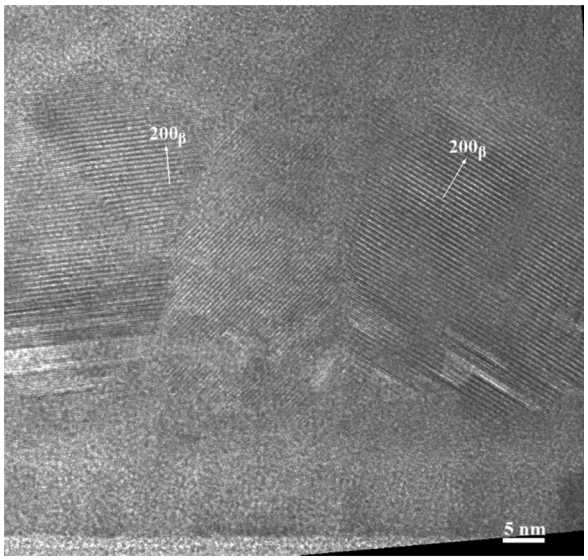

Fig. 6 HRTEM image showing the 0.59 nm lattice fringe, which was assigned to the (200) lattice planes of β-Ga_2O_3.

In contrast to the results of the present study, thin films of β-Ga_2O_3 were deposited by radio frequency magnetron sputtering on TiN with preferential (111) orientation[30] and on epitaxial Ru (0001).[31] Differences in seed-layer orientation and growth mechanisms were likely the main factors responsible for these dissimilarities.

3.2. Density, surface roughness, and growth rate

Results of XRR studies demonstrate that together with a T_G increase from 200 to 325 °C, the densities of films deposited on Ru and TiN bottom electrodes gradually increased (Fig. 7a). This increase in density was similar to that previously observed in the same T_G range for amorphous Ga_2O_3 films grown on bare Si substrates,[25,27] and was likely due to the increase in material purity related to the decrease of iodine content from 1.4 to 0.03 at% (Fig. 2). A more significant increase in the density of films deposited on Ru and TiN was observed with the increase of T_G from 325 to 375 °C that caused the transition from

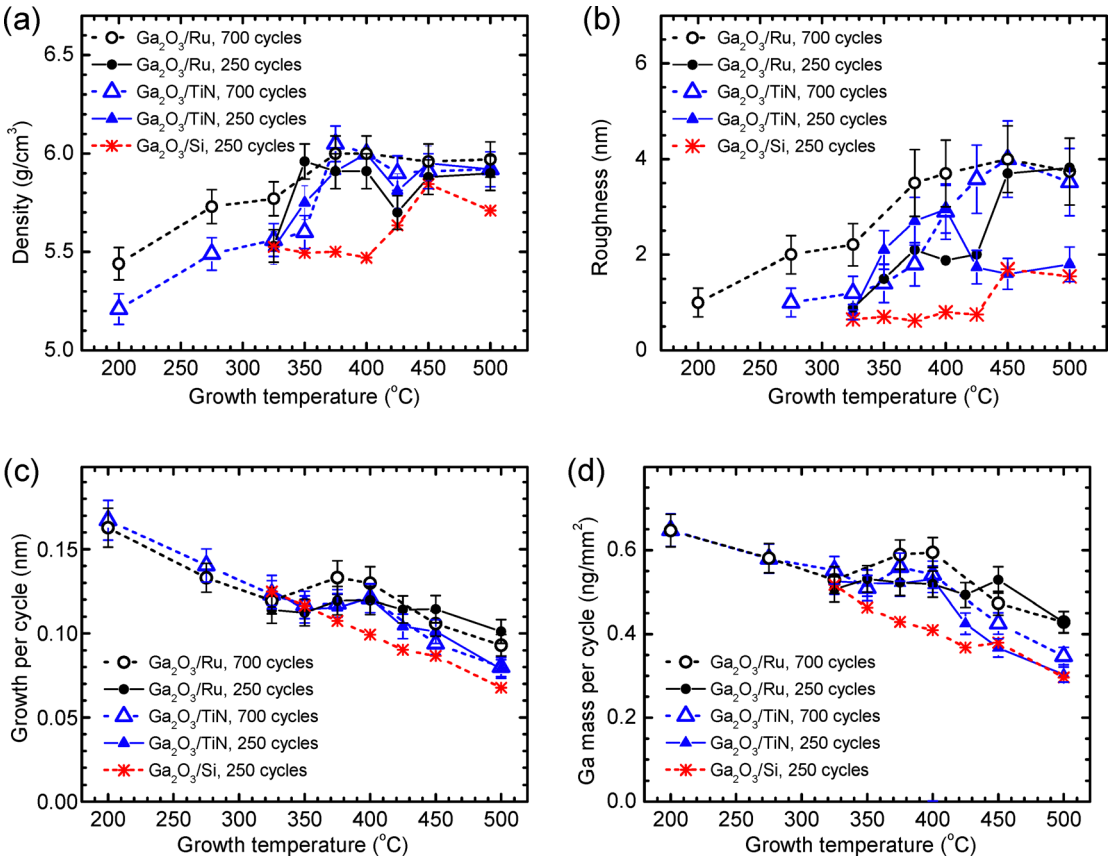

Fig. 7 (a) Density, (b) surface roughness, (c) thickness growth per cycle, and (d) Ga mass growth per cycle as a function of T_G for films grown with 250 ALD cycles on Ru, TiN, and Si, and with 700 ALD cycles on Ru and TiN.

amorphous to crystalline material growth (Fig. 3). As a result, the density increased to 5.96–6.05 g cm^{-3}, *i.e.*, close to the bulk density of single crystal κ-Ga_2O_3 (6.11 g cm^{-3}). Similar densities have been reported in XRD databases for ε-Ga_2O_3 (6.196 g cm^{-3}, PDF-2 file 01-082-3196) and in previous publications by Playford *et al.*[22] for ε-Ga_2O_3 (6.0622 g cm^{-3}) and Cora *et al.*[23] for κ-Ga_2O_3 (6.108 g cm^{-3}). In the case of films deposited on bare Si substrates, a density increase, attributable to the crystallization of the film material,[25,27] was observed with the increase of T_G from 400 to 450 °C (Fig. 7a). This result is in good agreement with the data of earlier studies.[25,27]

It is worth noting that in the T_G range of 325–450 °C, where the most significant changes in the density were observed (Fig. 7a), the influence of iodine impurities on the density could not be significant because of very low iodine concentrations ranging from 0.01 to 0.03 at% (Fig. 2). However, the low iodine concentration was a plausible reason why the crystal growth leading to the increase in the material density became possible.

The crystal growth also led to a significant increase in the surface roughness of films grown on Ru and TiN as well as on bare Si (Fig. 7b). As a result, the XRR roughness that was 0.6–1.0 nm in the case of amorphous films increased up to 3.7–4.0 nm when T_G increased to 450 °C (Fig. 7b). For comparison, the XRR roughness values of bare Si, Ru, and TiN surfaces were <0.5, 0.6 ± 0.1, and 1.0 ± 0.2 nm, respectively. Thus, the substrate roughness had a considerable direct effect only on the roughness of amorphous films. However, according to recent data of Baunthiyal *et al.*,[31] the surface roughness of Ru can enhance the nucleation of Ga_2O_3. This effect might also be a reason for rougher surfaces of amorphous films grown on Ru at 275 °C compared with those of similar films grown on TiN (Fig. 7b).

Considerable differences in the surface roughness of crystalline films grown on different substrates are at least partially related to the differences in the film thicknesses. Indeed, a comparison of results presented in Fig. 7b and c shows that the differences in the surface roughness are in correlation with differences in GPC. However, there is also a positive feedback between surface roughness and growth rate because higher surface roughness results in a higher specific surface area[43,44] and, correspondingly, higher amounts of precursors adsorbed during an ALD cycle.[25,27,44] This effect is one of the reasons for the increase in GPC (Fig. 7c) and Ga mass growth per cycle (Fig. 7d) with the increase in T_G leading to the crystal growth (Fig. 3).

An additional effect that can influence the growth rate is the difference in the reactivities of amorphous and crystalline materials towards the precursors, as discussed in previous publications.[25,27,43,44] Higher reactivity leads to more efficient

removal of precursor ligands in surface reactions and, correspondingly, an increase in the amount of film material adsorbed in an ALD cycle. The latter causes a proportional increase in the mass growth per cycle. Unfortunately, the separate determination of the contributions from surface roughness and reactivity to GPC is a complex task requiring measurement of specific surface area throughout the whole deposition process.[44] As this kind of very specific studies were not performed in this work, corresponding quantitative analysis was not possible. However, comparing the data presented in Fig. 7b and d, one can see that the changes in the Ga mass growth per cycle are in a very good correlation with corresponding changes in the surface roughness of crystalline films. Therefore, in the present case, the surface roughening seems to be the main reason for the higher growth rates of crystalline films.

3.3. Electrical properties

Electrical characterization of Pt/Ga_2O_3/Ru and Pt/Ga_2O_3/TiN structures demonstrated that symmetrical current–voltage (*I–V*) curves (Fig. 8) were typical for structures with amorphous and quasi-amorphous Ga_2O_3 layers deposited at T_G values up to 325 °C. Breakdown voltage amplitudes, recorded for these samples at different voltage polarities, were similar to each other (blue curves in Fig. 8a and b) while the breakdown electric field strengths (E_b) of these Ga_2O_3 films were 4.8–5.5 MV cm^{-1} (Fig. 9). The deposition of Ga_2O_3 at higher T_G caused an increase in the current recorded at the positive top-electrode voltage polarity, leading to the asymmetry of the *I–V* curves (Fig. 8). This result indicates that the potential barrier between the bottom electrode and Ga_2O_3 decreased with increasing T_G or the contribution of trap-assisted tunneling[45] increased due to the formation of a defective interface region at the bottom electrode. Based on the STEM scans (Fig. 1b and d) that revealed mixing of the bottom electrode materials with Ga_2O_3 at higher T_G, one can conclude that the growth of interface layers with graded composition was probably the main reason for both effects. Because of these changes in *I–V* curves, the E_b of the Ga_2O_3 layers deposited at $T_G \geq 350$ °C were reliably measurable only at the negative top-electrode biases (Fig. 8b).

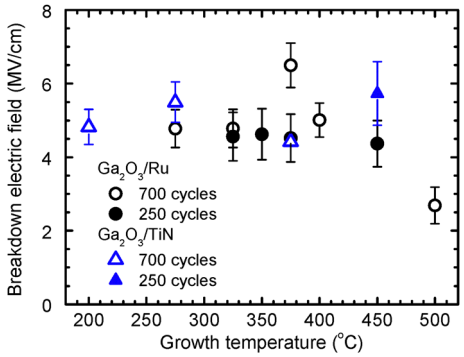

Fig. 9 Breakdown electric field strength as a function of T_G of Ga_2O_3 films deposited on Ru and TiN using 250 and 700 ALD cycles.

The highest E_b of 6.5 MV cm^{-1} (Fig. 9) was recorded for crystalline Ga_2O_3 deposited at 375 °C. Although E_b decreased to 2.7 MV cm^{-1} with the T_G increase to 500 °C (Fig. 9), all E_b values of our films were higher than those of around 1.2 and 2.0 MV cm^{-1}, reported for κ-Ga_2O_3 and (β + κ)-Ga_2O_3 films deposited on epitaxial Pt(1 1 1) bottom electrodes by metalorganic chemical vapor deposition (MOCVD), and plasma-enhanced ALD (PEALD).[21] Higher E_b values, for example, 6.5–7.6 MV cm^{-1} for amorphous Ga_2O_3,[14,15] 5.2–8.8 MV cm^{-1} for β-Ga_2O_3,[10,19,46,47] and 11 MV cm^{-1} for ultrathin (2.7–2.9 nm) native Ga_2O_3 grown on liquid metals,[48] can also be found in the literature. As a rule, the E_b values have been higher for Ga_2O_3 films deposited on Si or n$^+$-Ga_2O_3 substrates[10,46] than for the films with the same crystal structure grown on highly conductive bottom electrodes.[19,47] Comparing the parameters of films deposited on highly conductive substrates, the E_b values of 5.2 MV cm^{-1} for β-Ga_2O_3 transferred onto graphene[47] and 5.5 MV cm^{-1} for β-Ga_2O_3 deposited on Pt electrodes[19] can be found in the literature.

Therefore, the literature data and results depicted in Fig. 3 and 9 indicate that amorphous Ga_2O_3 (Fig. 9), β-Ga_2O_3,[19,47] and films that contain κ-Ga_2O_3 and ε-Ga_2O_3 (Fig. 9), all deposited on substrates with metallic conductivity, have comparable breakdown electric field strengths. As also shown in Fig. 9, the

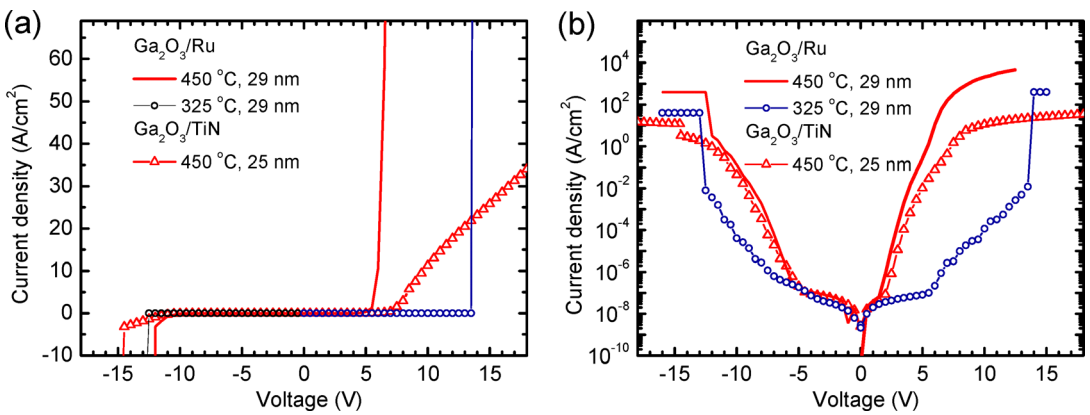

Fig. 8 Current density presented in (a) linear and (b) logarithmic scale as a function of voltage for Ga_2O_3 films deposited on Ru at 325 and 450 °C, and on TiN at 450 °C. The films were deposited using 250 ALD cycles. The film thicknesses are specified in the figure panels.

increase of T_G from 200 to 275 °C that resulted in the most significant decrease of the iodine content in amorphous films (Fig. 2) caused only a minor increase in the breakdown electric field strength (Fig. 9).

At low voltages and, thus, low-electric field strengths, the current densities recorded for crystalline films grown with 250 cycles at 375 °C and with 700 cycles at 325–400 °C were lower than those recorded at the same electric field strength for amorphous films grown with 250 cycles at 325 °C and with 700 cycles at 275 °C (Fig. 10, 11 and Fig. S7). At higher voltages, the current densities through crystalline Ga_2O_3 considerably exceeded that through amorphous Ga_2O_3 (Fig. 8). A possible reason for this effect is the diffusion of the bottom electrode materials into a Ga_2O_3 layer, causing an increase in the defect concentration and higher contribution of trap-assisted tunneling. Another reason for this difference is the higher surface roughness of crystalline films which increases the local electric field strength leading to higher probability of tunneling.

In the structures with thin Ga_2O_3 layers deposited on Ru electrodes at $T_G > 375$ °C, the leakage current density increased with T_G even at low voltages (Fig. 10a and 11). For example, a T_G increase from 450 to 500 °C caused an increase in the current density determined at an electric field strength of 0.1 MV cm^{-1} by 3 orders of magnitude (Fig. 11a and b). Assuming that thermionic emission controlled the current transport across the metal/dielectric interface at low electric field strengths,[49] a reduction of effective energetic barrier causing a comparable increase in current density was estimated to be about 0.2 eV. Since no such increase in the current density was observed in the case of thicker Ga_2O_3 layers (Fig. 10b and 11a, b), the effect can be related to the diffusion of Ru into Ga_2O_3 leading to a growth of more defective film material during the initial stage of deposition. In the thicker films grown using 700 ALD cycles, the contribution of the defective interface layer was evidently much smaller and therefore the increase in T_G did not cause a considerable increase in the current density (Fig. 11).

In the TEM image (Fig. 1a) and STEM-EDX scans (Fig. 1b) of the cross section of film deposited at 450 °C, a defective interface layer with a graded composition can be seen at the Ga_2O_3/Ru interface. The thickness of this layer ranged from 2 to 5 nm (Fig. 1a). Considering that at 500 °C an even thicker interface layer was formed, a significant effect of this layer on the *I–V* characteristics of a 25-nm-thick film is a predictable result. Although the influence of the interface layer on the leakage currents of 56-nm-thick films grown at 500 °C with

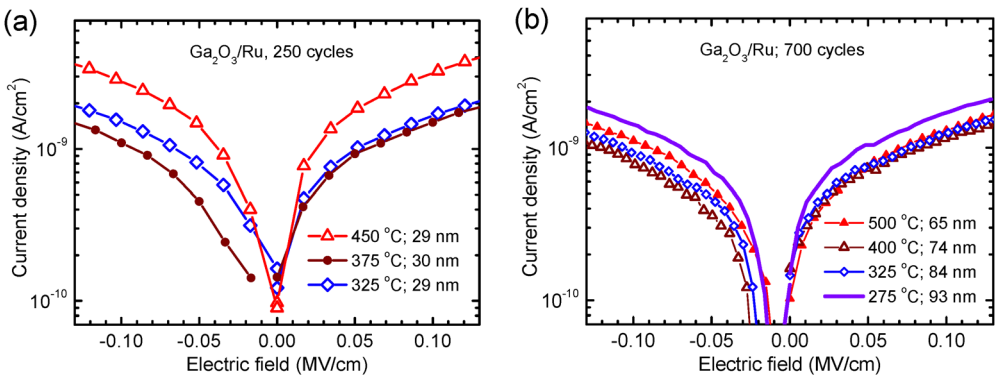

Fig. 10 Current density recorded as a function of electric field strength for Ga_2O_3 films deposited on Ru at different T_G using (a) 250 and (b) 700 ALD cycles. T_G and film thicknesses are shown in the figure panels.

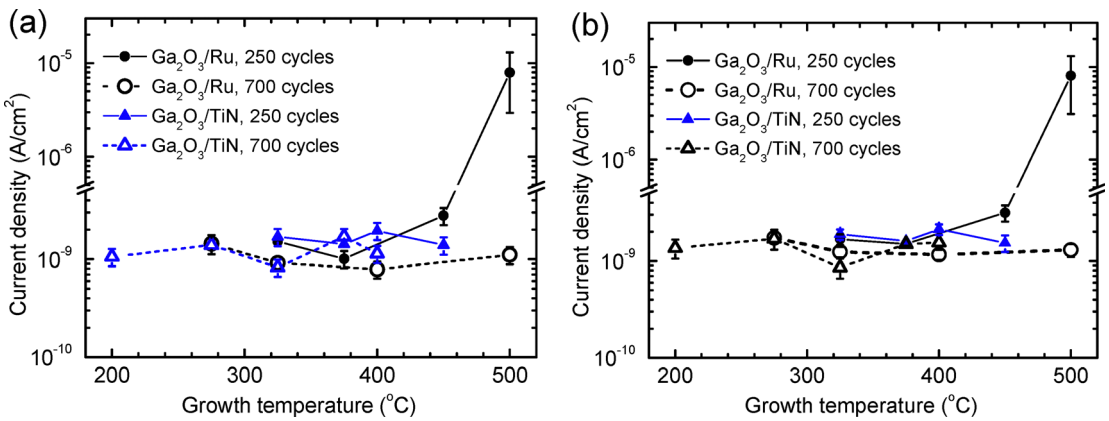

Fig. 11 Current densities measured at (a) negative and (b) positive top-electrode voltage polarities for Ga_2O_3 films deposited at 200–500 °C on Ru and TiN using 250 and 700 ALD cycles. The current densities were determined at an electric field strength of 0.1 MV cm^{-1}.

700 ALD cycles was expectedly weaker (Fig. 11), additional interface roughening related to the interface layer formation (Fig. 1a) evidently contributed to the reduction of the breakdown field with the increase of T_G to 500 °C (Fig. 9).

A notable result is the weak influence of T_G on the electrical characteristics of amorphous films obtained in the temperature range of 200–275 °C where the most considerable change in the concentration of residual iodine impurities occurred (Fig. 2). Thus, the role of these impurities in determining the charge carrier transport was not significant in the case of structures studied in this work.

The direct-current *I–V*-curves (Fig. 8a) and the data of alternate-current measurements showed that the series resistance of samples with Ga_2O_3 films deposited on TiN bottom electrodes at higher T_G was too high for reliable capacitance and permittivity measurements. A probable reason for this was the TiN oxidation during the ALD of Ga_2O_3 at higher T_G as can be concluded from the STEM-EDX line scans shown in Fig. 1d. Therefore, the results of permittivity measurements of the films grown on TiN are shown in Fig. 12 only for a limited T_G range. There was no such problem in the case of samples with Ru bottom electrodes because the RuO_2 formed on the surface of Ru (Fig. 1b) is conductive enough. Nevertheless, owing to the high leakage current densities of the Ga_2O_3 films deposited on Ru at 500 °C using 250 ALD cycles, accurate capacitance measurements of these films were not possible either.

The k values of Ga_2O_3, calculated from the capacitances measured at a frequency of 10 kHz, are depicted in Fig. 12. As can be seen, markedly higher k values were obtained for crystalline Ga_2O_3 films deposited at 375–500 °C than for the amorphous and quasi-amorphous films deposited at $T_G \leq$ 325 °C. The k values of 29–93 nm thick films containing κ-Ga_2O_3 and ε-Ga_2O_3 ranged from 15 to 22 at a frequency of 10 kHz, while the highest k was recorded for a 74 nm film deposited at 450 °C (Fig. 12).

The k values of our amorphous films, ranging from 13.0 to 14.2 (Fig. 12), were somewhat higher than the k of 9.2–11.9 published for amorphous Ga_2O_3 grown by ALD on Si substrates.[14,15] As the latter films showed higher breakdown fields,[14,15] it is possible that an interface SiO_2 layer that can easily be formed on the surface of Si in ALD processes[50] was responsible for the somewhat lower k and higher E_b of those.

The oxidation of the bottom TiN electrode also resulted in the underestimation of k in the case of our films because the formation of interfacial TiO_2 layer was not considered in the calculations of k. However, as the k of TiO_2[42] is higher than that of Ga_2O_3 (Fig. 12) and the thickness of an oxygen-rich region of TiO_xN_y formed on a TiN electrode at deposition temperatures up to 450 °C did not exceed 2 nm (Fig. 1d), the underestimation of k should not exceed 6% for 30-nm-thick Ga_2O_3 layers. In the case of thicker Ga_2O_3 films, this underestimation is even smaller. Therefore, the corresponding error in the determination of k is smaller than the experimental uncertainties shown in Fig. 12.

The k values determined at frequencies of 1–2 MHz for our amorphous and quasi-amorphous films deposited at 275–325 °C (Fig. 13) are comparable to those (up to 12.4) determined for single-crystal β-Ga_2O_3 at 1 MHz[17] and 0.2–1 THz.[17,18] By contrast, the k values of films that contained κ-Ga_2O_3 and ε-Ga_2O_3 grown at $T_G \geq$ 375 °C in our experiments (Fig. 12 and 13) significantly exceeded the values reported for β-Ga_2O_3,[17–19] being well comparable to k reported for orthorhombic Ga_2O_3.[20,21]

Significant variation of k values, similar to that recorded for our films containing orthorhombic Ga_2O_3, has also been observed in earlier studies. For instance, Yuza *et al.*[20] reported k values of 15 and 32 at 10 kHz for orthorhombic films with the thicknesses 89 and 136 nm, respectively. At the same frequency, He *et al.*[21] obtained k = 18 for a 700 nm thick MOCVD film predominantly containing κ-Ga_2O_3, and k = 27 for a 50 nm thick PEALD film containing mixed κ-Ga_2O_3 and β-Ga_2O_3 phases. The latter result, showing that k values determined for a mixture of phases is much higher than the k of any component of the mixture, is somewhat surprising and requires further study. An explanation proposed by He *et al.*[21] was that the MOCVD films, showing lower k, also contained considerable amounts of

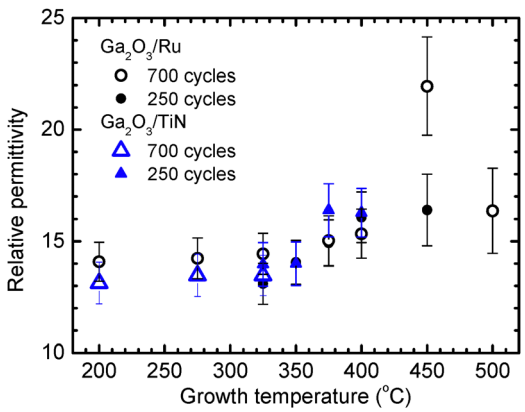

Fig. 12 Relative permittivity determined at a frequency of 10 kHz as a function of T_G for Ga_2O_3 films deposited on Ru and TiN using 250 and 700 ALD cycles.

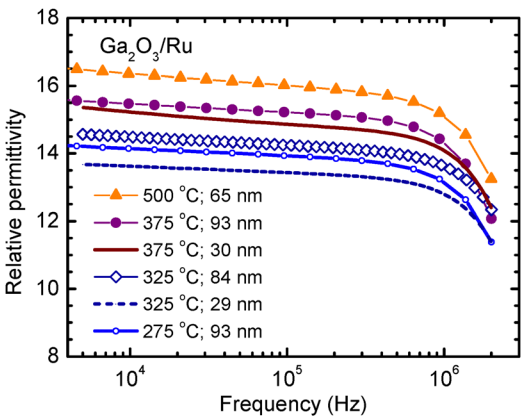

Fig. 13 Relative permittivity determined as a function of frequency for Ga_2O_3 films deposited on Ru at different T_G. T_G and film thicknesses are specified in the figure panel.

β-Ga_2O_3, but due to the location of β-Ga_2O_3 at the film–substrate interface, its effect on the data of electrical measurements was stronger than the influence on the XRD results.

Results of XRD and TEM studies indicated that some amounts of β-Ga_2O_3 were also present in the films deposited in our experiments at 450 °C (Fig. 3, 6 and Fig. S2). However, the T_G increase from 450 °C to higher temperatures, causing an increase in the intensity of the XRD reflections attributable to β-Ga_2O_3 (Fig. 3 and Fig. S2), led to a decrease in k (Fig. 12). Therefore, the formation of β-Ga_2O_3 together with κ/ε-Ga_2O_3 does not seem to be the main reason for obtaining high k in our studies.

The marked differences in k, measured for Ga_2O_3 films, can also be related to dissimilar concentrations of oxygen vacancies in the films. For instance, in a recent study, k values as high as 18.1–20.8 at 10 kHz were reported for 3–7-μm-thick aerosol-deposited β-Ga_2O_3 films.[19] However, annealing of these films at 800 °C under oxygen-containing ambient conditions resulted in a decrease of k to 8.8–9.3, that is, to the values that are more common for β-Ga_2O_3. Simultaneously the leakage current through the dielectric decreased and the breakdown field increased from 1–2 MV cm^{-1} to 5.5 MV cm^{-1}.[19] Based on these results, Lee *et al.*[19] concluded that high concentration of oxygen vacancies was the reason for the very high k obtained for aerosol-deposited films before annealing at high-temperature. In our experiments, in contrast, the increase of T_G from 325 to 400 °C for thinner films and from 325 to 450 °C for thicker films, leading to the increase in k (Fig. 12 and 13), did not cause corresponding decrease in breakdown electric field (Fig. 9) and an increase in leakage current (Fig. 11). Thus, the relatively high k values of our films (Fig. 12 and 13) were not due to a high concentration of oxygen vacancies.

The possible contribution of residual iodine impurities to k also seems to be insignificant because no correlation between these two parameters could be found. In particular, k did not vary considerably when the iodine concentration decreased from 1.4 to 0.03 at% with the increase of T_G from 200 to 325 °C (Fig. 2 and 12). Instead, k most significantly increased with T_G in a temperature range of 350–450 °C where iodine concentration variations did not exceed 0.02 at%. Consequently, the predominant growth of κ-Ga_2O_3 together with inclusions of ε-Ga_2O_3 is the main reason for the high k of films deposited at 375–450 °C in our studies.

Unfortunately, due to the structural similarities of κ-Ga_2O_3 and ε-Ga_2O_3, finding the process parameters for separate growing each of these two phases and clarifying the individual contribution of each phase to the electrical properties of Ga_2O_3 thin films is a task that requires additional investigation. Nevertheless, the results of our study already demonstrate that the films containing these phases have promising dielectric properties for the application of those in capacitor structures and gate stacks of field effect transistors. In addition, the ALD process based on GaI_3 and O_3 as precursors is suitable for growing these films on the Ru and TiN surfaces at relatively low T_G. However, because of the detrimental effect of GaI_3 and O_3 on the substrate surfaces, especially at higher temperatures, careful selection of process parameters is of significant importance in the implementation of this ALD process.

4. Conclusions

This study shows that the ALD process based on GaI_3 and O_3 as precursors allows the growth of Ga_2O_3 films with high breakdown electric field strength and permittivity values. Crystalline Ga_2O_3 with a predominant κ-Ga_2O_3 phase was formed in the films deposited on Ru and TiN seed layers at temperatures down to 325 °C. In addition, minor amounts of ε-Ga_2O_3 and β-Ga_2O_3 were found in the films by TEM studies. A comparison of Ga_2O_3 deposition on Ru and TiN with that on Si indicated that the formation of crystalline phases in the films caused a considerable increase in growth per cycle and an expected increase in the density and surface roughness. The effect of crystallization on the breakdown electric field and leakage current density was weak. At the same time, the highest breakdown field (6.5 MV cm^{-1}) and the lowest leakage current densities (1.0–1.1 nA cm^{-2} at a mean electric field of 0.1 MV cm^{-1} applied to the Pt/Ga_2O_3/TiN structure) were recorded for crystalline Ga_2O_3. The relative permittivity determined at a frequency of 10 kHz reached values up to 14 in the case of amorphous films, deposited at 275 °C, and up to 22 in the case of κ/ε-Ga_2O_3 films deposited on Ru at 450 °C. These results demonstrate that the GaI_3–O_3 ALD process can be applied for deposition of high-quality Ga_2O_3 films on both Ru and TiN bottom electrodes. It should further be noted that, at higher temperatures, this ALD process has a detrimental effect on the concerned electrodes. A marked increase in the resistance of TiN appeared because of its oxidation while, at $T_G > 450$ °C, the degradation of Ga_2O_3/Ru interface properties, related to the diffusion of Ru into the Ga_2O_3 layer, caused a decrease in the breakdown voltage and increase in the leakage current density.

Author contributions

The manuscript was written through contributions from all authors. All authors have given approval to the final version of the manuscript.

Conflicts of interest

The authors declare that there are no financial or any other types of conflicts of interest to declare for this submission.

Data availability

Data are available from the authors upon request.

Supplementary information (SI) is available. See DOI: https://doi.org/10.1039/d5tc04544d.

Acknowledgements

The authors are thankful to Alma-Asta Kiisler for the technical assistance. The research was funded by the Estonian Research Council (grant PRG2594) and the Estonian Ministry of Education and Research through the Center of Excellence in Sustainable Green Hydrogen and Energy Technologies (grant TK210U5).

References

1 B. R. Tak, S. Kumar, A. K. Kapoor, D. Wang, X. Li, H. Sun and R. Singh, Recent advances in the growth of gallium oxide thin films employing various growth techniques—a review, *J. Phys. D: Appl. Phys.*, 2021, **54**, 453002, DOI: 10.1088/1361-6463/ac1af2.

2 X.-Q. Zheng, H. Zhao and P. X.-L. Feng, A perspective on β-Ga_2O_3 micro/nanoelectromechanical systems, *Appl. Phys. Lett.*, 2022, **120**, 040502, DOI: 10.1063/5.0073005.

3 B. Li, Y. Wang, Z. Luo, W. Xu, H. Gong, T. You, X. Ou, J. Ye, Y. Hao and G. Han, Gallium oxide (Ga_2O_3) heterogeneous and heterojunction power devices, *Fundam. Res.*, 2025, **5**, 804–817, DOI: 10.1016/j.fmre.2023.10.008.

4 W. Wu, H. Huang, Y. Wang, H. Yin, K. Han, X. Zhao, X. Feng, Y. Zeng, Y. Zou, X. Hou, Z. Wei and S. Long, Structure engineering of Ga_2O_3 photodetectors: a review, *J. Phys. D: Appl. Phys.*, 2025, **58**, 063003, DOI: 10.1088/1361-6463/ad902f.

5 A. Moore, S. Rafique, C. Llewelyn, D. Lamb and L. Li, A review of Ga_2O_3 heterojunctions for deep-UV photodetection: current progress, methodologies, and challenges, *Adv. Electron. Mater.*, 2025, 2400898, DOI: 10.1002/aelm.202400898.

6 M. Pavesi, F. Fabbri, F. Boschi, G. Piacentini, A. Baraldi, M. Bosi, E. Gombia, A. Parisini and R. Fornari, ε-Ga_2O_3 epilayers as a material for solar-blind UV photodetectors, *Mater. Chem. Phys.*, 2018, **205**, 502–507, DOI: 10.1016/j.matchemphys.2017.11.023.

7 X. Chen, W. Mi, J. Wu, Z. Yang, K. Zhang, J. Zhao, C. Luan and Y. Wei, A solar-blind photodetector based on β-Ga_2O_3 film deposited on MgO(100) substrates by RF magnetron sputtering, *Vacuum*, 2020, **180**, 109632, DOI: 10.1016/j.vacuum.2020.109632.

8 S. An, S. Park, Y. Mun and C. Lee, UV enhanced NO_2 sensing properties of Pt functionalized Ga_2O_3 nanorods Bull, *Korean Chem. Soc.*, 2013, **34**, 6, DOI: 10.5012/bkcs.2013.34.6.1632.

9 J. Zhu, Z. Xu, S. Ha, D. Li, K. Zhang, H. Zhang and J. Feng, Gallium oxide for gas sensor applications: a Comprehensive Review, *Materials*, 2022, **15**, 7339, DOI: 10.3390/ma15207339.

10 J.-S. Li, C.-C. Chiang, X. Xia, H.-H. Wan, F. Ren and S. J. Pearton, Effect of drift layer doping and NiO parameters in achieving 8.9 kV breakdown in 100 μm diameter and 4 kV/4 A in 1 mm diameter NiO/β-Ga_2O_3 rectifiers, *J. Vac. Sci. Technol., A*, 2023, **41**, 043404, DOI: 10.1116/6.0002722.

11 P. Bokemeyer, C. Petersen, C. Dethloff, Y. Chen, H. von Wenckstern, M. Grundmann and S. Vogt, α-Ga_2O_3-based heterojunction diodes and junction field-effect transistors, *Phys. Status Solidi RRL*, 2025, 2400388, DOI: 10.1002/pssr.202400388.

12 K. Sato, Y. Hayashi and N. Masaoka, *et al.*, High-temperature operation of gallium oxide memristors up to 600 K, *Sci. Rep.*, 2023, **13**, 1261, DOI: 10.1038/s41598-023-28075-4.

13 H. Ohta, K. Nomura, H. Hiramatsu, K. Ueda, T. Kamiya, M. Hirano and H. Hosono, Frontier of transparent oxide semiconductors, *Solid-State Electron.*, 2003, (47), 2261, DOI: 10.1016/S0038-1101(03)00208-9.

14 D.-W. Choi, K.-B. Chung and J.-S. Park, Low temperature Ga_2O_3 atomic layer deposition using gallium tri-isopropoxide and water, *Thin Solid Films*, 2013, **546**, 31–34, DOI: 10.1016/j.tsf.2013.03.066.

15 X. Li, H.-L. Lu, H.-P. Ma, J.-G. Yang, J.-X. Chen, W. Huang, Q. Guo, J.-J. Feng and D. W. Zhang, Chemical, optical, and electrical characterization of Ga_2O_3 thin films grown by plasma-enhanced atomic layer deposition, *Curr. Appl. Phys.*, 2019, **19**, 72–81, DOI: 10.1016/j.cap.2018.11.013.

16 S. J. Pearton, J. Yang, P. H. Cary IV, F. Ren, J. Kim, M. J. Tadjer and M. A. Mastro, A review of Ga_2O_3 materials, processing, and devices, *Appl. Phys. Rev.*, 2018, **5**, 011301, DOI: 10.1063/1.5006941.

17 A. Fiedler, R. Schewski, Z. Galazka and K. Irmscher, Static dielectric constant of β-Ga_2O_3 perpendicular to the principal planes (100), (010), and (001), *ECS J. Solid State Sci. Technol.*, 2019, **8**, Q3083–Q3085, DOI: 10.1149/2.0201907jss.

18 P. Gopalan, S. Knight, A. Chanana, M. Stokey, P. Ranga, M. A. Scarpulla, S. Krishnamoorthy, V. Darakchieva, Z. Galazka, K. Irmscher, A. Fiedler, S. Blair, M. Schubert and B. Sensale-Rodriguez, The anisotropic quasi-static permittivity of single-crystal *β*-Ga_2O_3 measured by terahertz spectroscopy, *Appl. Phys. Lett.*, 2020, **117**, 252103, DOI: 10.1063/5.0031464.

19 J.-W. Lee, J. H. Won, W. Kim, J.-B. Jeon, M.-Y. Cho, S. Kim, M. Kim, C. Park, W. H. Shin, K. Won, S.-M. Koo and J.-M. Oh, Ultrahigh breakdown field in gallium(III) oxide dielectric structure fabricated by novel aerosol deposition method, *Small Struct.*, 2024, **5**, 2400321, DOI: 10.1002/sstr.202400321.

20 S. Yusa, D. Oka and T. Fukumura, High-κ dielectric stabilized in a transparent heteroepitaxial structure grown by mist CVD at atmospheric pressure, *CrystEngComm*, 2020, **22**, 381–385, DOI: 10.1039/c9ce01532a.

21 F. He, K. Jiang, Y. Choi, B. L. Aronson, S. Shetty, J. Tang, B. Liu, Y. Liu, K. P. Kelley, G. B. Rayner, R. F. Davis, L. M. Porter and S. Trolier-McKinstry, High field dielectric response in κ-Ga_2O_3 films, *J. Appl. Phys.*, 2023, **134**, 204101, DOI: 10.1063/5.0169420.

22 H. Y. Playford, A. C. Hannon, E. R. Barney and R. I. Walton, Structures of uncharacterized polymorphs of gallium oxide from total neutron diffraction, *Chem. – Eur. J.*, 2013, **19**, 2803–2813, DOI: 10.1002/chem.201203359.

23 I. Cora, F. Mezzadri, F. Boschi, M. Bosi, M. Čaplovičová, G. Calestani, I. Dódony, B. Pécz and R. Fornari, The real structure of ε-Ga_2O_3 and its relation to κ-phase, *CrystEngComm*, 2017, **19**, 1509–1516, DOI: 10.1039/c7ce00123a.

24 E. Dobročka, F. Gucmann, K. Hušeková, P. Nádaždy, F. Hrubišák, F. Egyenes, A. Rosová, M. Mikolášek and

M. Ťapajna, Structure and Thermal Stability of ε/κ-Ga_2O_3 Films Deposited by Liquid-Injection MOCVD, *Materials*, 2023, **16**, 20, DOI: 10.3390/ma16010020.

25 L. Aarik, H. Mändar, J. Kozlova, A. Tarre and J. Aarik, Atomic Layer Deposition of Ga_2O_3 from GaI_3 and O_3: Growth of high-density phases, *Cryst. Growth Des.*, 2023, **23**(8), 5899–5911, DOI: 10.1021/acs.cgd.3c00502.

26 T. Oshima, T. Nakazono, A. Mukai and A. Ohtomo, Epitaxial growth of γ-Ga_2O_3 films by mist chemical vapor deposition, *J. Cryst. Growth*, 2012, **359**, 60–63, DOI: 10.1016/j.jcrysgro.2012.08.025.

27 L. Aarik, H. Mändar, A. Kasikov, A. Tarre and J. Aarik, Optical properties of Ga_2O_3 thin films grown by atomic layer deposition using GaI_3 and O_3 as precursors, *J. Mater. Chem. C*, 2024, **12**, 10562, DOI: 10.1039/d4tc01846j.

28 S. Ilhom, A. Mohammad, D. Shukla, J. Grasso, B. G. Willis, A. K. Okyay and N. Biyikli, Low-temperature as-grown crystalline β-Ga_2O_3 films via plasma-enhanced atomic layer deposition, *ACS Appl. Mater. Interfaces*, 2021, **13**, 8538–8551, DOI: 10.1021/acsami.0c21128.

29 Q. Cao, L. He, H. Xiao, X. Feng, Y. Lv and J. Ma, β-Ga_2O_3 epitaxial films deposited on epi-GaN/sapphire (0001) substrates by MOCVD, *Mater. Sci. Semicond. Process.*, 2018, **77**, 58–63, DOI: 10.1016/j.mssp.2018.01.010.

30 C.-C. Yen, A. K. Singh, P.-W. Wu, H.-Y. Chou and D.-S. Wuu, Interface engineering in epitaxial growth of sputtered β-Ga_2O_3 films on Si substrates via TiN(111) buffer layer for Schottky barrier diodes, *Mater. Today Adv.*, 2023, **17**, 100348, DOI: 10.1016/j.mtadv.2023.100348.

31 A. Baunthiyal, M. Schowalter, M. Williams, J.-O. Krisponeit, T. Mehrtens, A. Karg, A. Rosenauer, M. Eickhoff and J. Falta, Structural evolution and nucleation dynamics of RF sputtered Ga_2O_3 films on Ru(0001): the impact of deposition temperature and Ru surface morphology, *APL Mater.*, 2025, **13**, 041130, DOI: 10.1063/5.0270431.

32 H. Nishinaka, D. Tahara and M. Yoshimoto, Heteroepitaxial growth of ε-Ga_2O_3 thin films on cubic (111) MgO and (111) yttria-stablized zirconia substrates by mist chemical vapor deposition, *Jpn. J. Appl. Phys.*, 2016, **55**, 1202BC, DOI: 10.7567/JJAP.55.1202BC.

33 Y. Oshima, E. Víllora, Y. Matsushita, S. Yamamoto and K. Shimamura, Epitaxial growth of phase-pure ε-Ga_2O_3 by halide vapor phase epitaxy, *J. Appl. Phys.*, 2015, **118**, 085301, DOI: 10.1063/1.4929417.

34 F. Boschi, M. Bosi, T. Berzina, E. Buffagni, C. Ferrari and R. Fornari, Hetero-epitaxy of ε-Ga_2O_3 layers by MOCVD and ALD, *J. Cryst. Growth*, 2016, **443**, 25–30, DOI: 10.1016/j.jcrysgro.2016.03.013.

35 V. Gottschalch, S. Merker, S. Blaurock, M. Kneiß, U. Teschner, M. A. Grundmann and H. Krautscheid, Heteroepitaxial growth of α-, β-, γ- and κ-Ga_2O_3 phases by metalorganic vapor phase epitaxy, *J. Cryst. Growth*, 2019, **510**, 76–84, DOI: 10.1016/j.jcrysgro.2019.01.018.

36 H. Nishinaka, H. Koma, D. Tahara, Y. Arata and M. Yoshimoto, Microstructures and rotational domains in orthorhombic ε-Ga_2O_3 thin films, *Jpn. J. Appl. Phys.*, 2018, **57**, 115601, DOI: 10.7567/JJAP.57.115601.

37 T. Kato, H. Nishinaka, K. Shimazoe, K. Kanegae and M. Yoshimoto, Demonstration of bixbyite-structured δ-Ga_2O_3 thin films using β-Fe_2O_3 buffer layers by mist chemical vapor deposition, *ACS Appl. Electron. Mater.*, 2023, **5**, 1715–1720, DOI: 10.1021/acsaelm.2c01750.

38 J. Aarik, T. Arroval, L. Aarik, R. Rammula, A. Kasikov, H. Mändar, B. Hudec, K. Hušekova and K. Fröhlich, Atomic layer deposition of rutile-phase TiO_2 on RuO_2 from $TiCl_4$ and O_3: growth of high-permittivity dielectrics with low leakage current, *J. Cryst. Growth*, 2013, **382**, 61–66, DOI: 10.1016/j.jcrysgro.2013.08.006.

39 L. Aarik, T. Arroval, P. Ritslaid, A. Vask, H. Mandar and J. Aarik, Influence of substrates on structure development and concentration of residual impurities in hafnium–titanium-oxide films grown by atomic layer deposition, *Cryst. Growth Des.*, 2023, **23**, 548–557, DOI: 10.1021/acs.cgd.2c01174.

40 J. Aarik, A. Aidla, A. Jaek, M. Leskelä and L. Niinistö, In situ study of a strontium β-diketonate precursor for thin film growth by atomic layer epitaxy, *J. Mater. Chem.*, 1994, **4**, 1239–1244, DOI: 10.1039/JM9940401239.

41 M. Klinger, More features, more tools, more CrysTBox, *J. Appl. Crystallogr.*, 2017, **50**, 1226–1234, DOI: 10.1107/S1600576717006793.

42 K. Fröhlich, M. Ťapajna, A. Rosová, E. Dobročka, K. Hušeková, J. Aarik and A. Aidla, Growth of high-dielectric-constant TiO_2 films in capacitors with RuO_2 electrodes, *Electrochem. Solid State Lett*, 2008, **11**(6), G19–G21, DOI: 10.1149/1.2898184.

43 J. Aarik, A. Aidla, H. Mändar and V. Sammelselg, Anomalous effect of temperature on atomic layer deposition of titanium dioxide, *J. Cryst. Growth*, 2000, **220**, 531–537, DOI: 10.1016/S0022-0248(00)00897-6.

44 J. Aarik, J. Karlis, H. Mändar, T. Uustare and V. Sammelselg, Influence of structure development on atomic layer deposition of TiO_2 thin films, *Appl. Surf. Sci.*, 2001, **181**, 339–348, DOI: 10.1016/S0169-4332(01)00430-5.

45 J. Racko, M. Mikolášek, L. Harmatha, J. Breza, B. Hudec, K. Fröhlich, J. Aarik, A. Tarre, R. Granzner and F. Schwierz, Analysis of leakage current mechanisms in RuO_2–TiO_2–RuO_2 MIM structures, *J. Vac. Sci. Technol., B*, 2011, **29**, 01AC08, DOI: 10.1116/1.3534022.

46 A. Kaya, H. Mao, J. Gao, R. V. Chopdekar, Y. Takamura, S. Chowdhury and M. S. Islam, An investigation of electrical and dielectric parameters of sol–gel process enabled *β*-Ga_2O_3 as a gate dielectric material, *IEEE Trans. Electron Devices*, 2017, **64**, 2047–2053, DOI: 10.1109/TED.2017.2675990.

47 X. Yan, I. S. Esqueda, J. Ma, J. Tice and H. Wang, High breakdown electric field in β-Ga_2O_3/graphene vertical barrister heterostructure, *Appl. Phys. Lett.*, 2018, **112**, 032101, DOI: 10.1063/1.5002138.

48 K. Yi, W. Qin, Y. Huang, Y. Wu, S. Feng, Q. Fang, X. Cao, Y. Deng, C. Zhu, X. Zou, K.-W. Ang, T. Li, X. Wang, J. Lou,

K. Lai, Z. Hu, Z. Zhang, Y. Dong, K. Kalantar-Zadeh and Z. Liu, Integration of high-κ native oxides of gallium for two-dimensional transistors, *Nat. Electron.*, 2024, **7**, 126–1136, DOI: 10.1038/s41928-024-01286-x.

49 C. Hou, R. M. Gazoni, R. J. Reeves and M. W. Allen, Direct comparison of plain and oxidized metal Schottky contacts on β-Ga_2O_3, *Appl. Phys. Lett.*, 2019, **114**, 033502, DOI: 10.1063/1.5079423.

50 D. R. G. Mitchell, J. Aarik and A. Aidla, Transmission electron microscopy studies of HfO_2 thin films grown by chloride-based atomic layer deposition, *Appl. Surf. Sci.*, 2006, **253**, 606–617, DOI: 10.1016/j.apsusc.2005.12.133.